Stem Cell Reports
Article

ISSCR

OPEN ACCESS

Suppressing Nodal Signaling Activity Predisposes Ectodermal Differentiation of Epiblast Stem Cells

Chang Liu,[1] Ran Wang,[1] Zhisong He,[2] Pierre Osteil,[3] Emilie Wilkie,[3,4] Xianfa Yang,[1,5] Jun Chen,[1] Guizhong Cui,[1] Wenke Guo,[1,5] Yingying Chen,[1,5] Guangdun Peng,[1] Patrick P.L. Tam,[3,6] and Naihe Jing[1,5,*]

[1]State Key Laboratory of Cell Biology, CAS Center for Excellence in Molecular Cell Science, Shanghai Institute of Biochemistry and Cell Biology, Chinese Academy of Sciences, University of Chinese Academy of Sciences, 320 Yue Yang Road, Shanghai 200031, China
[2]CAS Key Laboratory of Computational Biology, CAS-MPG Partner Institute for Computational Biology, Shanghai 200031, China
[3]Embryology Unit, Children's Medical Research Institute, Westmead, NSW 2145, Australia
[4]Bioinformatics Group, Children's Medical Research Institute, Westmead, NSW 2145, Australia
[5]School of Life Science and Technology, ShanghaiTech University, 100 Haike Road, Shanghai 201210, China
[6]School of Medical Sciences, Sydney Medical School, University of Sydney, Westmead, NSW 2145, Australia
*Correspondence: njing@sibcb.ac.cn
https://doi.org/10.1016/j.stemcr.2018.05.019

SUMMARY

The molecular mechanism underpinning the specification of the ectoderm, a transient germ-layer tissue, during mouse gastrulation was examined here in a stem cell-based model. We captured a self-renewing cell population with enhanced ectoderm potency from mouse epiblast stem cells (EpiSCs) by suppressing Nodal signaling activity. The transcriptome of the Nodal-inhibited EpiSCs resembles that of the anterior epiblast of embryonic day (E)7.0 and E7.5 mouse embryo, which is accompanied by chromatin modifications that reflect the priming of ectoderm lineage-related genes for expression. Nodal-inhibited EpiSCs show enhanced ectoderm differentiation *in vitro* and contribute to the neuroectoderm and the surface ectoderm in postimplantation chimeras but lose the propensity for mesendoderm differentiation *in vitro* and in chimeras. Our findings show that specification of the ectoderm progenitors is enhanced by the repression of Nodal signaling activity, and the ectoderm-like stem cells provide an experimental model to investigate the molecular characters of the epiblast-derived ectoderm.

INTRODUCTION

Mouse gastrulation is a rapid and dynamic process that commences following the formation of the postimplantation embryo, which is made up of the epiblast and visceral endoderm derived from the inner cell mass of the blastocyst, and the extra embryonic ectoderm derived from the trophectoderm. During gastrulation, at embryonic day (E) 6.5 to E7.5, epiblast cells are allocated to the primitive streak for the generation of the mesoderm and definitive endoderm (Lu et al., 2001), whereas cells remaining in the epiblast are endowed the ectoderm property (Tam and Loebel, 2007). Fate mapping the E7.5 late-gastrula mouse embryo revealed that the anterior epiblast is predisposed for neural and surface ectoderm cell fates (Tam, 1989). Clonal analysis has further revealed the presence of bipotential progenitors in the anterior epiblast of E7.0 mid-gastrula embryo (Cajal et al., 2012) that can differentiate into both neural and epidermal lineage *in vitro* (Li et al., 2013). These findings are consistent with the concept that the anterior epiblast of the gastrulating embryo harbors the ectoderm progenitors.

The process of specification and commitment of the ectoderm lineage in developing embryo is less well understood. The paucity of molecular markers that signify the emergence of the lineage and the lack of appropriate experimental model for studying the biology of ectoderm progenitor cells have impeded our understanding of the development of the ectoderm lineage. In particular, there is an unfulfilled requirement for an *in vitro* cell-based model for studying ectoderm development. Pluripotent stem cells (PSCs) have been isolated from mouse embryos, such as the embryonic stem cells (ESCs) from the epiblast of preimplantation blastocyst (Evans and Kaufman, 1981; Martin, 1981), and the epiblast stem cells (EpiSCs) (Brons et al., 2007; Kojima et al., 2014; Tesar et al., 2007) and "region-selective" EpiSCs (rsEpiSCs) (Wu et al., 2015) from the postimplantation epiblast. None of these stem cell types, however, consistently display predisposed ectoderm lineage potency.

During gastrulation, Nodal and Wnt signaling play pivotal roles on the formation of the primitive streak, progression of gastrulation, and tissue patterning in the anterior-posterior axis of the embryo. The spatial transcriptome study and analysis of gene-expression domain of the gastrula stage mouse embryo revealed that cells in different regions of the epiblast are subject to different levels of Nodal and Wnt signaling (Peng et al., 2016; Pfister et al., 2007). Nodal signaling is active in the posterior epiblast for primitive streak formation and mesendoderm development (Brennan et al., 2001; Conlon et al., 1994). In contrast, the anterior epiblast that is fated for the ectoderm appears to be a "signal-silent" zone for Nodal activity through genome-wide study (Peng et al., 2016). Canonical

Wnt-β-catenin signaling is required for axis formation and mesoderm induction in the mouse embryo. In the loss of *Wnt3* (Liu et al., 1999) and β-catenin mutants (Huelsken et al., 2000), mesoderm fails to form. The repression of Wnt signaling activity by the antagonist, such as DKK1 emanating from anterior visceral endoderm, is associated with the acquisition of ectoderm potency by the anterior epiblast (Kimura-Yoshida et al., 2005). Loss of Dkk1 function, which creates a gain of Wnt function, leads to the loss of brain and cranial structures (Lewis et al., 2008; Mukhopadhyay et al., 2001), which could be related to an altered ectoderm potency of neural progenitor tissue. These findings imply that a diminished level of Nodal and Wnt signaling activity may underpin the acquisition of the ectoderm lineage potency.

Consistent with the concept that suppressing Nodal signaling enables the acquisition of ectoderm cell fates, blocking Nodal signaling promotes neural ectoderm differentiation of human ESCs *in vitro* (Li et al., 2011; Patani et al., 2009; Smith et al., 2008; Vallier et al., 2004), and double-mutant embryos of Nodal antagonists *Cer1* and *Lefty1* result in the loss of neural ectoderm and the ectopic differentiation of mesoderm (Perea-Gomez et al., 2002). Loss of Nodal function leads to precocious neural differentiation and early loss of pluripotency of the epiblast (Camus et al., 2006; Mesnard et al., 2006). In mouse EpiSCs, blocking activin signaling enhances neural differentiation (Brons et al., 2007; Tesar et al., 2007; Vallier et al., 2009). An ectoderm-like state can be induced in the mouse ESC-derived EpiSCs (ESD-EpiSCs) by Nodal inhibition (Li et al., 2015). However, these ectoderm-like cells are unstable and do not self-renew *in vitro*.

In this study, we tested whether modulation of the Nodal and Wnt signaling activity may impact on the lineage potency of the mouse EpiSCs that were derived and maintained under fibroblast growth factor 2 (FGF2)/activin A conditions. Our findings showed that inhibiting Wnt activity has no discernible effect of the lineage propensity of the established EpiSCs, while inhibiting Nodal activity can enhance the ectoderm lineage propensity. Nodal-inhibited EpiSCs differentiate efficiently to cells of the epidermis lineage *in vitro* while retaining the neuroectoderm potential, but these cells lose the ability to differentiate into mesendoderm derivatives.

RESULTS

Inhibiting WNT Signaling Activity in Epiblast Stem Cells Has No Impact on Lineage Propensity

EpiSCs were derived from the epiblast of the E6.5 early-primitive-streak-stage mouse embryo and maintained in culture supplemented with FGF2 and activin A. To assess the impact of abrogating WNT activity on the lineage property of the established EpiSC, we added a chemical inhibitor (IWP2), which blocks WNT signaling by inhibiting the function of Porcupine that mediates the trafficking and secretion of WNT ligand (Gao and Hannoush, 2014), to the culture for over ten passages (IW-EpiSC) (Figure S1A). To characterize the differentiation potency of these EpiSCs, we assessed the expression profile of lineage markers over 4 days of *in vitro* differentiation by microfluidic qPCR. The EpiSC and IW-EpiSC showed similar patterns of lineage differentiation *in vitro* in terms of the relative number of germ-layer-specific genes that were expressed at days 0 and 4 and the trajectory of lineage differentiation (Figures S1B and S1C). These findings suggest that abrogating WNT activity did not rewire the lineage property of EpiSCs. However, IW-EpiSCs in activin A-containing medium were potentially still subject to transforming growth factor β (TGF-β) signaling activity, such as Nodal, which may counteract any effect elicited by the inhibition of WNT activity on lineage propensity. We therefore proceeded to test the effect of inhibiting Nodal activity on the EpiSCs.

Derivation of EpiSCs$^{S/F}$ from EpiSCs

We tested the effect of blocking Nodal pathway using SB431542 (SB43) (Figure 1A), which inhibits the activity of TGF-β receptors. SB43-treated EpiSCs cultured in chemical defined medium (CDM) only (without activin A and FGF2) showed extensive cell death (Figure 1B), whereas those cultured in CDM supplemented with FGF2 formed epithelial colonies (Figure 1B). From these colonies, a stable EpiSC line (denoted as EpiSCs$^{S/F}$) that self-renewed for over 40 passages was derived and maintained in CDM + FGF2 + SB43. Another EpiSC$^{S/F}$ line was also derived from EpiSCs generated from the epiblast of 129 strain E5.5 mouse embryo (Figures S1D and S1E). EpiSCs$^{S/F}$ can also be derived from single cells from the parental EpiSC line (Figure S1F). EpiSCs$^{S/F}$ could be reverted back to the EpiSC state by withdrawing SB43 and culturing in EpiSCs medium (denoted EpiSC$^{SF\text{-}AF}$). EpiSCs$^{SF\text{-}AF}$ showed morphology and transcriptome profiles similar to those of EpiSCs (Figures 1C–1E), indicating that the EpiSCs$^{S/F}$ have not been hard-wired to an SB/F-specific status.

Immunocytochemistry revealed that the expression of the pluripotent factors, SOX2 and OCT4, was comparable between EpiSCs and EpiSCs$^{S/F}$ (Figure 2A, upper panels), while single-cell PCR results showed a lower average mRNA level of *Oct4* in EpiSCs$^{S/F}$ compared with EpiSCs (Figure 2B). EpiSCs$^{S/F}$ showed weaker alkaline phosphatase activity than ESCs and EpiSCs (Figure S2A), but proliferated at rates as similar to those of EpiSCs (Figure S2B). qRT-PCR analysis revealed that Nodal downstream target genes were suppressed in EpiSCs$^{S/F}$ (Figure S2C). qPCR analysis revealed that treatment with SB43 induced a rapid repression

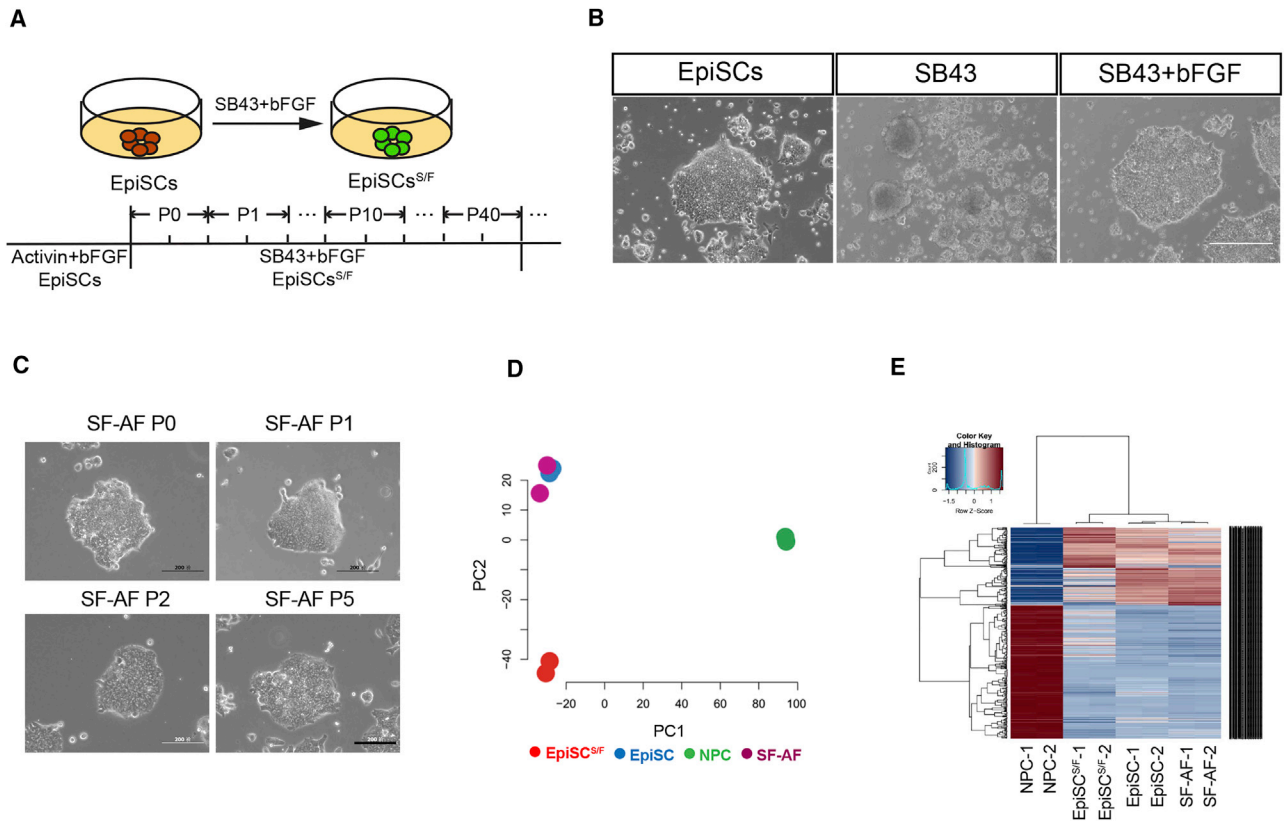

Figure 1. Derivation of EpiSC$^{S/F}$ from EpiSCs

(A) Strategy for EpiSCs$^{S/F}$ production. P, passage.

(B) EpiSCs on feeder-free culture in three different media supplemented with activin A and bFGF, SB43 only, and SB43 plus bFGF, respectively. Phase-contrast images. Scale bar, 500 μm.

(C) Morphology of EpiSC$^{S/F}$ cultured in activin A and bFGF supplemented medium (SF-AF). Scale bar, 200 μm.

(D) PCA display of RNA-seq data of EpiSCs$^{S/F}$, EpiSCs, SF-AF, and neural progenitor cells (NPCs).

(E) Hierarchical clustering of EpiSCs$^{S/F}$, EpiSCs, SF-AF, and NPCs.

of *Fgf5* expression during EpiSCs$^{S/F}$ derivation (Figures S2D and S2E). Analysis of *Oct4*, *Otx2*, *T*, *Sox1*, and *Ck18* at different passages (Figures 2B and S2E), further showed that the EpiSC$^{S/F}$ maintained a stable phenotype on extended passaging.

To characterize the EpiSCs$^{S/F}$, we compared the transcriptome of EpiSCs$^{S/F}$ with that of EpiSCs derived with activin-FGF2 (Kojima et al., 2014) and the ESC-derived EpiSCs. Hierarchical clustering analysis of the transcriptome showed that EpiSCs$^{S/F}$ were grouped separately from EpiSCs and ESC-derived EpiSCs (Zhang et al., 2010) (Figure S3A). The expression of EpiSC markers (*Nanog*, *T*, *Fgf5*, *Eomes*, and *Lefty1*) was lower in EpiSCs$^{S/F}$ (Figure 2A, middle panels; Figure S2F). EpiSCs and EpiSCs$^{S/F}$ expressed similar level of junctional gene E-CADHERIN and anterior epiblast marker OTX2, but EpiSCs$^{S/F}$ showed higher expression of another anterior epiblast marker, SIX3 (Figure 2A, lower panels). Both EpiSCs and EpiSCs$^{S/F}$ did not express the markers of ESCs (*Rex1*, *Esrrb*, and *Klf4*), and very low level of markers of mesendoderm cells (*Flk1*, *Gata6*, and *Sox17*), neural progenitor cells (NPCs) (*Pax6*, *Zfp521*, and *Nestin*), and epidermis (*Ck18*, *Ck19*, *Ck8* and *Grhl2*) (Figure S2F).

Taken together, stable EpiSC$^{S/F}$ cell lines can be derived from established EpiSCs by inhibiting Nodal signaling, and these self-renewing cells are molecularly distinctive from naive (ESC) and primed pluripotent stem cells (EpiSCs) as well as three tissue progenitor cells.

EpiSC$^{S/F}$ Exhibit Gene-Expression Profiles that Are Similar to the Ectoderm of Late-Mid-Streak-Stage Embryos

Compared with EpiSCs, genes that were highly expressed in EpiSCs$^{S/F}$ are related to neural and epithelium development. In contrast, genes related to gastrulation and endoderm differentiation were more highly expressed in

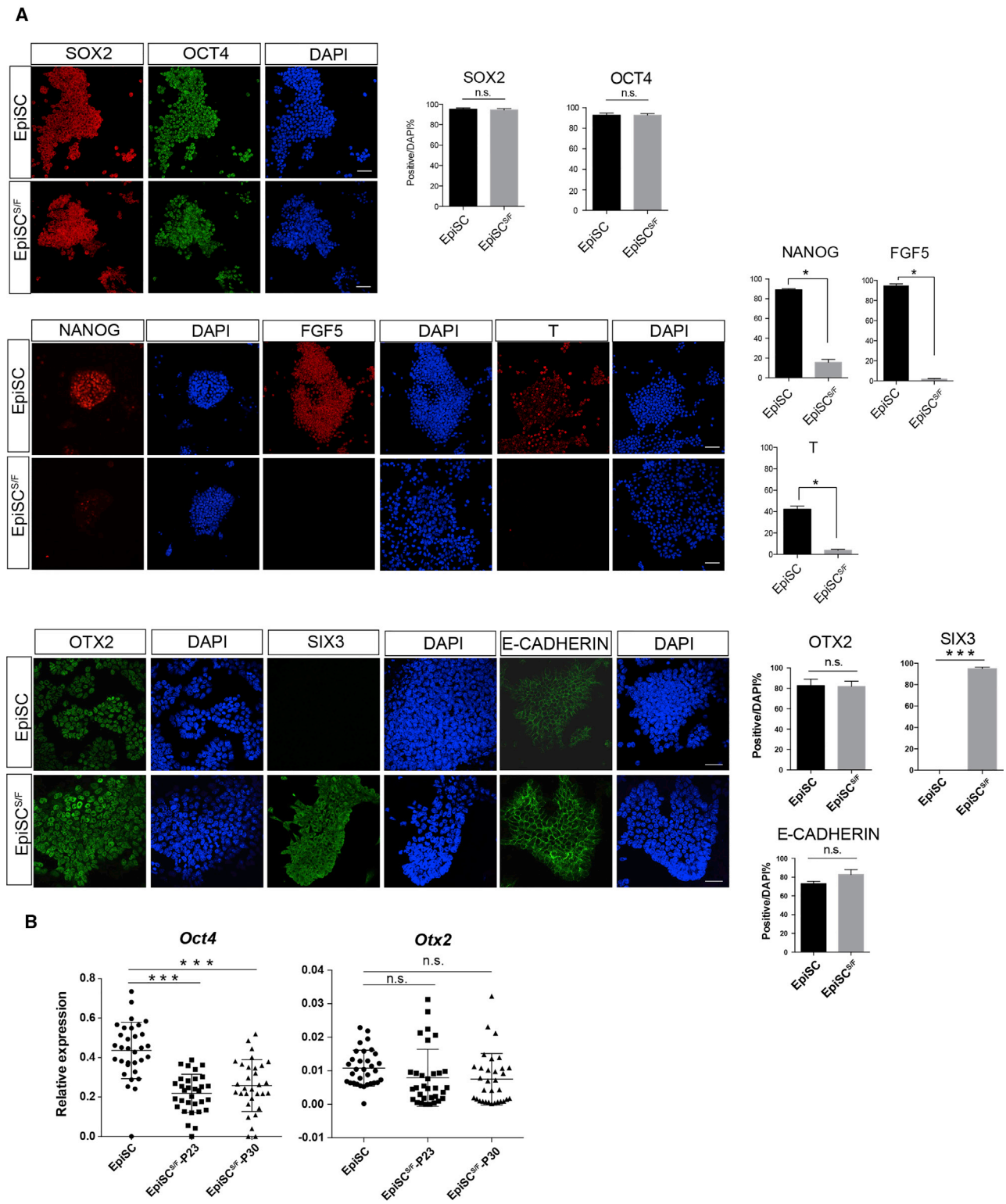

Figure 2. Characterization of EpiSC$^{S/F}$

(A) Expression of SOX2 and OCT4 (upper panels), NANOG, FGF5, and T (middle panels), and OTX2, SIX3, and E-CADHERIN (lower panels) in EpiSCs$^{S/F}$ and EpiSCs. Immunofluorescence and DAPI counterstaining. *$p < 0.05$, ***$p < 0.001$, significant difference in the fraction of cells

(legend continued on next page)

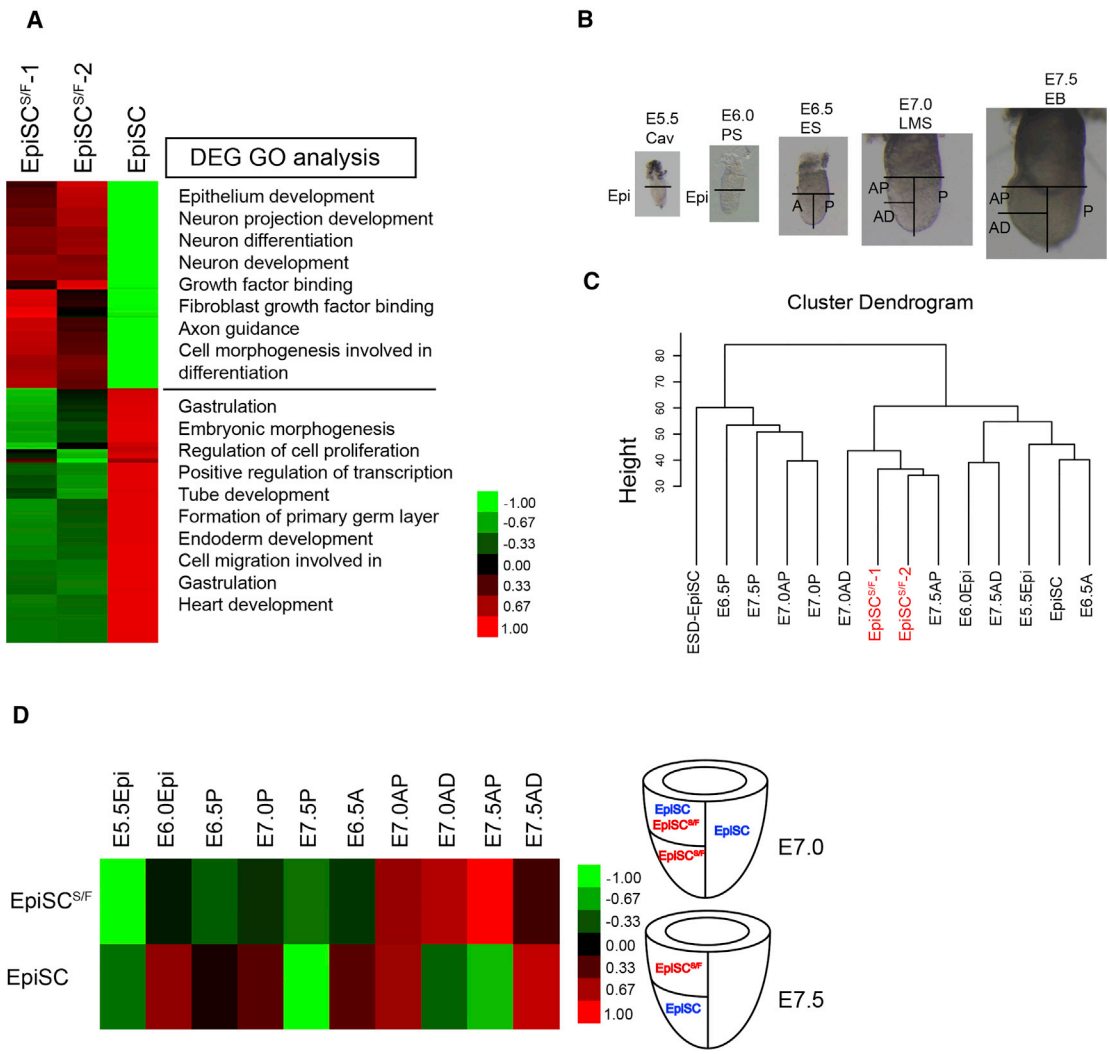

Figure 3. Developmental Correlates of EpiSCs$^{S/F}$

(A) Gene ontology (GO) analysis of differentially expressed genes (DEG) in EpiSC and EpiSC$^{S/F}$.

(B) Epiblast/ectoderm samples for RNA-seq from E5.5 (cavity stage, Cav), E6.0 (prestreak stage, PS), E6.5 (early-streak stage, ES), E7.0 (late-middle streak stage, LMS), and E7.5 (early-bud stage, EB) mouse embryos. A, anterior; P, posterior; Epi, epiblast; AP, anterior proximal; AD, anterior distal.

(C) Hierarchical clustering by the transcriptome of EpiSCs$^{S/F}$ (as technical replicates, red), EpiSCs, ESD-EpiSCs, and epiblast/ectoderm samples.

(D) Pearson correlation analysis of EpiSCs$^{S/F}$ and EpiSCs with embryonic tissue samples for matching the EpiSC and EpiSC$^{S/F}$ to the epiblast/ectoderm of E5.5 to E7.5 embryos.

EpiSCs (Figure 3A). To delineate the *in vivo* epiblast counterpart of the EpiSC$^{S/F}$, we compared the transcriptome of the EpiSC$^{S/F}$ with that of the epiblast sampled from embryonic parts of the cavity stage (E5.5) to early-bud stage (E7.5) embryos (Figure 3B). Hierarchical clustering, principal component analysis (PCA), and Pearson

displaying positive immunofluorescence (% positive/DAPI) by Student's t test, n = 5 samples for each type of EpiSC. n.s., not significant. Scale bars, 50 μm.

(B) qPCR analysis of the expression of *Oct4* and *Otx2* in EpiSCs and EpiSCs$^{S/F}$ (at passages 23 and 30). Thirty cells per cell type were analyzed by qPCR. Statistical analysis was performed using Student's t test (***p < 0.001; n.s., not significant).

Data are means ± SD.

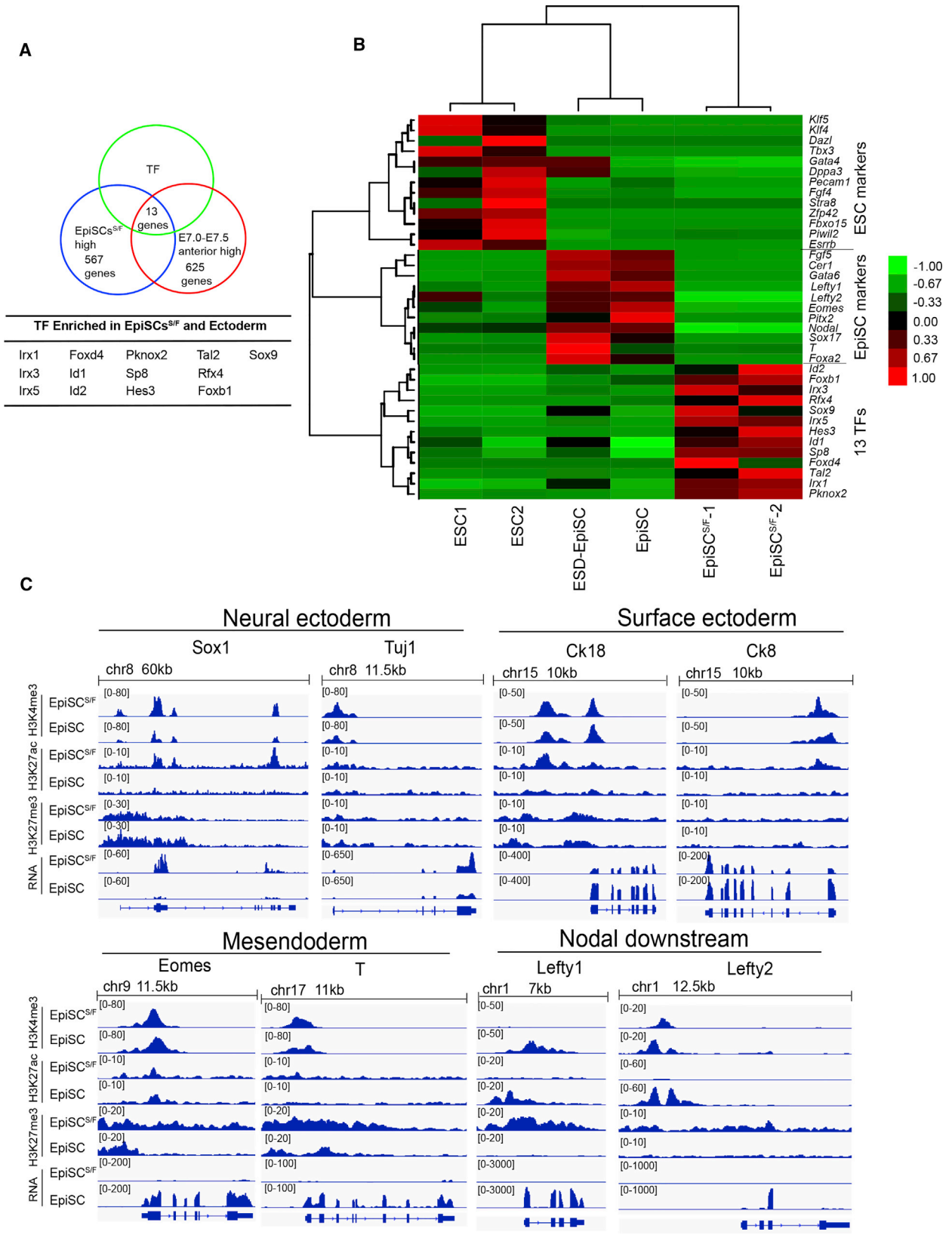

(legend on next page)

correlation analysis showed that EpiSCs$^{S/F}$ resembled most the anterior ectoderm of E7.0 and E7.5 embryo (Figures 3C, 3D, and S3B). In contrast, the parental EpiSCs are broadly similar to the epiblast of E6.5 embryo, the posterior epiblast of E7.0 embryo, and anterior epiblast of E7.5 embryo. To collate genes that may uniquely identify the EpiSCs$^{S/F}$, we analyzed genes that showed high expression in both EpiSCs$^{S/F}$ and E7.0–E7.5 anterior ectoderm, and found 13 commonly enriched transcription factors (TFs) (Figure 4A). These 13 TF genes were expressed exclusively in EpiSCs$^{S/F}$ and not in ESCs and EpiSCs (Buecker et al., 2014; Tesar et al., 2007) (Figure 4B). EpiSC$^{S/F}$ thus represents a unique type of EpiSCs that may resemble the anterior ectoderm of the advanced gastrula embryo.

To elucidate the chromatin characteristics of EpiSC$^{S/F}$, we surveyed the genome-wide pattern of H3K27 acetylation (H3K27ac), H3K27 trimethylation (H3K27me3), and H3K4 trimethylation (H3K4me3) in comparison with EpiSC. H3K27ac and H3K4me3, which marked active promoters, were detected in the promoter region of many genes in both EpiSC$^{S/F}$ and EpiSC (Figure S4A).

We further characterized the histone modifications on lineage markers. In EpiSC$^{S/F}$, active chromatin modifications (high H3K4me3, high H3K27ac, low H3K27me3) were found in the promoter of neural ectoderm marker genes (*Sox1*, *Tuj1*), surface ectoderm marker genes (*Ck18*, *Ck8*), and ectoderm-related genes (*Id1*, *Id2*) (Figures 4C and S4B). Mesendoderm marker genes (*Eomes* and *T*) that were expressed more highly in EpiSCs showed bivalent modifications (high H3K4me3, high H3K27me3) in EpiSCs$^{S/F}$ (Figure 4C). Consistent with the RNA sequencing (RNA-seq) data, Nodal downstream genes (*Lefty1* and *Lefty2*) showed repressive modification (low H3K4me3, low H3K27ac, high H3K27me3) in EpiSC$^{S/F}$ (Figure 4C). These results on the epigenetic marks suggested that ectoderm lineage genes may be at an open to active state following the transition from EpiSC to EpiSC$^{S/F}$. For the mesendoderm lineage genes, histone modifications were changed from active to bivalent status in the EpiSCs$^{S/F}$. These changes in histone modifications are consistent with the enhanced surface ectoderm potential and diminished mesendoderm potential of EpiSCs$^{S/F}$, and may reflect the interplay for signaling and intrinsic programs during EpiSC$^{S/F}$ derivation.

Taken together, the correlation of epigenomic modification and the switch to ectoderm propensity point to the role of ectoderm-poised chromatin modification in mediating the ectoderm propensity of EpiSCs$^{S/F}$.

EpiSCs$^{S/F}$ Behaved Like Anterior Ectoderm Progenitors in Chimeras

To test the differentiation potential of EpiSCs$^{S/F}$ in an embryonic context, we assessed the contribution of EpiSCs$^{S/F}$ to germ-layer derivatives in postimplantation chimeras (Huang et al., 2012; Kojima et al., 2014; Mascetti and Pedersen, 2016; Wu et al., 2015). RFP-expressing EpiSCs and EpiSCs$^{S/F}$ were grafted to anterior (Ant), distal (Dis), and posterior (Post) regions of the epiblast of E6.5 embryo (Figure 5A), and the distribution of the graft-derived cells was examined after 48 hr of *in vitro* culture. A site-specific pattern of tissue distribution was observed (Figure 5B). EpiSCs stayed as clumps, whereas EpiSCs$^{S/F}$ showed proliferation and incorporation when grafted to the anterior epiblast (Figures 5B–5D). EpiSCs$^{S/F}$ grafted into distal and posterior sites showed a much lower level of incorporation and cell proliferation (Figures 5B–5D). Immunostaining data showed that both EpiSCs$^{S/F}$ and EpiSC-derived cells expressed the appropriate neuroectoderm marker (SOX2) and surface ectoderm marker (CK18). In contrast, EpiSC$^{S/F}$-derived cells did not express mesendoderm markers such as FOXA2 and TBX6 (Figures 5E and 5F). When grafted into the E7.0 embryo (Figure S5A), both EpiSCs and EpiSCs$^{S/F}$ remained unincorporated when grafted to the anterior epiblast (Figure S5B), whereas EpiSCs$^{S/F}$ grafted into post sites showed similar frequency of incorporation but a lower level of cell proliferation than EpiSCs (Figures S5C and S5D). Collectively, the findings of chimera assay suggest that EpiSC$^{S/F}$ has acquired the developmental attribute that is compatible with the anterior epiblast of E6.5 embryo, and show ectoderm differentiation potential in the chimeras. While the EpiSCs$^{S/F}$ were similar transcriptome-wise to the E7.0 and E7.5 anterior ectoderm, they were developmentally incompatible when enforced to differentiate in the tissue environment of the E7.0 host embryo. Whether this is

Figure 4. Gene Expression and Epigenetic Signature of EpiSC$^{S/F}$

(A) Transcription factors that are enriched in the transcriptome of the anterior ectoderm and the EpiSCs$^{S/F}$.

(B) Heatmap of the expression of transcription factor (TF) genes of ESCs, EpiSCs (technical replicates), and anterior ectoderm in ESCs, ESD-EpiSCs, EpiSCs, and EpiSCs$^{S/F}$.

(C) Histone modifications and the expression (RNA) of selected lineage marker genes neural ectoderm (*Sox1*), surface ectoderm (*Ck18*), mesendoderm (*Eomes*), and Nodal and downstream (*Lefty1*) in EpiSCs and EpiSCs$^{S/F}$. For each gene, first panel: H3K4me3 signal; second panel: H3K27ac signal; third panel: H3K27me3 signal around transcription start site in EpiSCs and EpiSCs$^{S/F}$. The last panel shows RNA expression level in EpiSCs and EpiSCs$^{S/F}$.

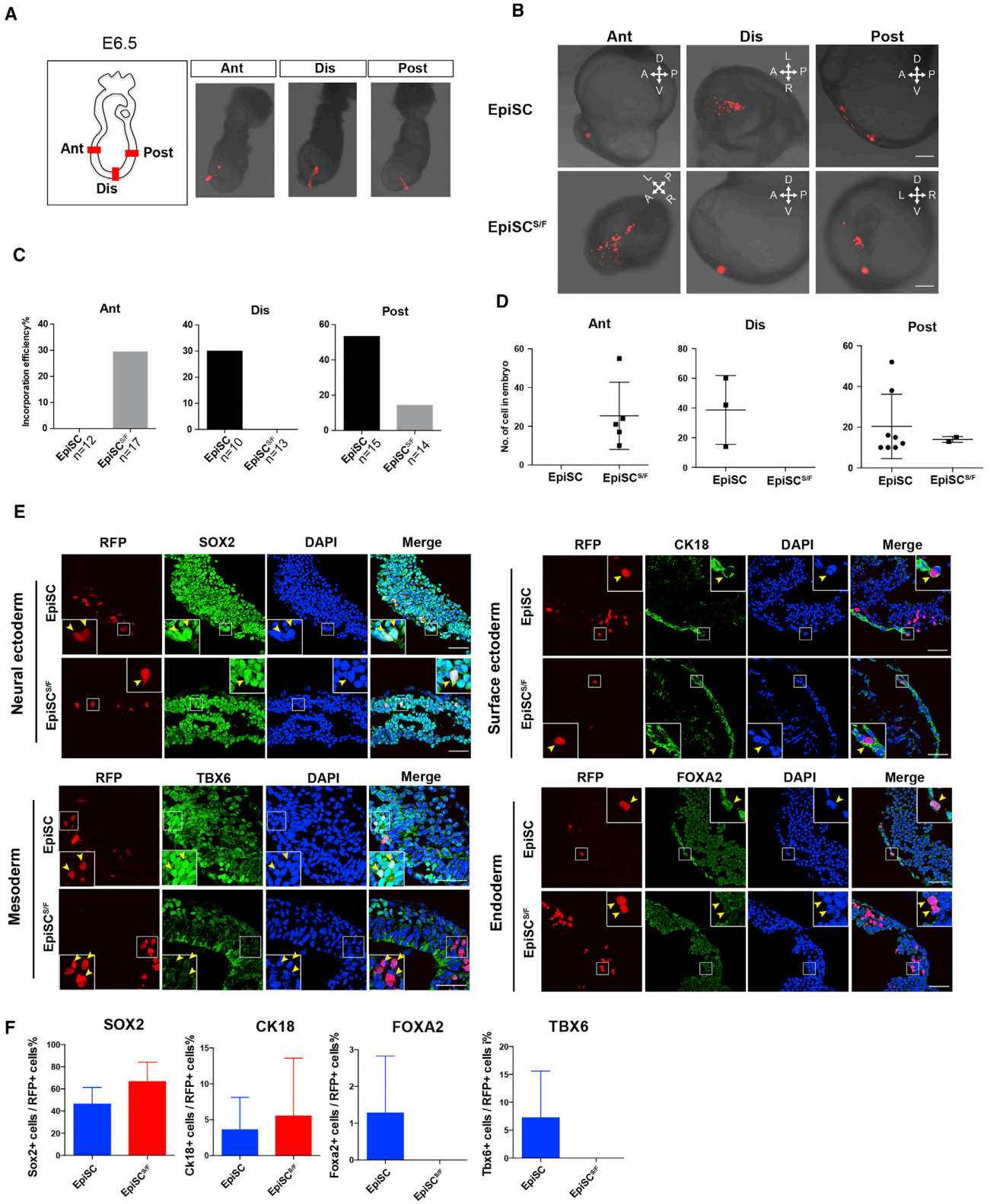

(legend on next page)

underpinned by the developmental asynchrony of EpiSCs$^{S/F}$ and the host environment is presently not known.

EpiSC$^{S/F}$ Display Propensity of Ectoderm Differentiation

To assess the lineage potential, we generated embryoid bodies (EBs) from the EpiSCs and cultured in the presence of bone morphogenetic protein (BMP) that promote differentiation of the neuroectoderm, or in the absence of BMP for epidermis and mesendoderm differentiation (Zhu et al., 2014). EpiSC$^{S/F}$ EBs showed higher expression of *Sox1* (a neural marker) than EpiSC EBs (Figure 6A, upper panels), but not early NPC markers such as *Zfp521* and *Nestin* (Figure 6A, upper panels). In BMP4-supplemented medium, EpiSC$^{S/F}$ EBs displayed stronger expression of *Ck18*, *Ck8*, and *CK19* (epidermis markers) than EpiSC EBs (Figure 6A, middle panels). In contrast, BMP4 did not induce the expression of *Flk1*, *Gata6*, and *Sox17* (mesoderm and endoderm markers) in EpiSC$^{S/F}$ EBs (Figure 6A, lower panels). Immunostaining showed that similar population of cells in EpiSC$^{S/F}$ EBs and EpiSC EBs (at day 4 of differentiation in BMP-free medium) expressed neural markers (TUJ1 and NESTIN), but more EpiSCs$^{S/F}$ expressed epidermal markers (CK18 and CK8) (Figure 6B). Relative to EpiSCs, fewer EpiSCs$^{S/F}$ expressed the mesoderm markers: FLK1 and NKX2.5 in BMP-supplemented medium (Figure 6B) and *Foxa2*, *Sox17*, *Flk1*, and *Gsc* in serum-containing medium (Figure 6C).

We further assessed the ectoderm propensity of EpiSC$^{S/F}$ by studying the differentiation of a single-cell colony of EpiSCs and EpiSCs$^{S/F}$ in culture medium with or without BMP4 for 24 hr. More single cells in the EpiSC$^{S/F}$ clones displayed higher expression of neural markers (*Sox1*, *Nestin*) and epidermis markers (*Ck18*, *Ck8*) compared with those of EpiSC clones. Very low expression of mesendoderm marker *T* and *Eomes* was found in single cells from EpiSC$^{S/F}$ after 24 hr of differentiation *in vitro* (Figure 6D). These results showed that EpiSCs$^{S/F}$ are more responsive to directed ectoderm differentiation but less amenable to mesendoderm differentiation.

DISCUSSION

Here, we report the derivation of a unique type of self-renewing EpiSCs, the EpiSCs$^{S/F}$, which display a distinctive molecular signature of ectoderm lineage propensity. Recent studies have shown that the functional attributes of stem cells *in vitro* can be modulated by signaling activity that are known to influence lineage fates *ex vivo*. For instance, EpiSCs, which are derived by culturing epiblast in FGF2 and activin A, acquire the molecular property of anterior primitive streak (Kojima et al., 2014) whereby embryonic cells *in vivo* are subject to strong Nodal signaling. As a result of extended exposure to activin A, EpiSCs may lose the ability to differentiate into primordial germ cells (PGCs), but EpiLCs generated by transient differentiation of ESCs retain the capacity to respond to WNT and BMP induction of PGCs (Hayashi et al., 2012). Consistent with the fact that *ex vivo* ectoderm differentiation of the epiblast can be enhanced by suppressing Nodal signaling (Li et al., 2013), blocking Nodal signaling in EpiSCs enables the derivation of EpiSC$^{S/F}$ cell lines that are poised for ectoderm differentiation. The gene-expression profile of these cells matches the cells in the anterior ectoderm of E7.0/E7.5 embryo that are fated for ectoderm differentiation. EpiSC$^{S/F}$ may therefore represent a cellular state when the pluripotent epiblast transits to the progenitors of neural and surface ectoderm.

Our finding highlights the feasibility of generating lineage-specific stem cell lines by mimicking the signaling condition in the embryo for *in vitro* derivation and maintenance of EpiSCs. The EpiSC$^{S/F}$ shows an enhanced surface ectoderm propensity but a diminished propensity for mesendoderm differentiation, which is coincidental with the

Figure 5. Differentiation of EpiSC$^{S/F}$ in Postimplantation Chimeras

(A) RFP-expressing EpiSC$^{S/F}$ and EpiSC grafted to anterior (Ant), distal (Dis), and posterior (Post) regions of the epiblast of E6.5 embryo.

(B) Distribution of graft-derived cells in host embryo 48 hr after transplantation of RFP-expressing cells in anterior (Ant), distal (Dis), and posterior (Post) regions of embryo. Scale bar, 200 μm.

(C) Percentage of host embryos showing the incorporation of graft-derived cells. n = 12 embryos for EpiSC and n = 17 embryos for EpiSC$^{S/F}$ in anterior (Ant) grafted group. n = 10 embryos for EpiSC and n = 13 embryos for EpiSC$^{S/F}$ in distal (Dis) grafted group. n = 15 embryos for EpiSC and n = 14 embryos for EpiSC$^{S/F}$ in posterior (Post) grafted group.

(D) Number of EpiSC- and EpiSC$^{S/F}$-derived cells in the host embryo. Data are mean ± SD, no error estimation for groups with "zero" score. n = 5 embryos for EpiSC and n = 5 embryos for EpiSC$^{S/F}$ in anterior (Ant) grafted group. n = 3 embryos for EpiSC and n = 3 embryos for EpiSC$^{S/F}$ in distal (Dis) grafted group. n = 8 embryos for EpiSC and n = 5 embryos for EpiSC$^{S/F}$ in posterior (Post) grafted group.

(E) Expression of lineage markers in chimeras detected by immunostaining Arrowheads mark cells of interest. Scale bars, 50 μm.

(F) Percentage of SOX2$^+$ cells, CK18$^+$ cells, FOXA2$^+$ cells, and TBX6$^+$ cells in the RFP-positive cell population in the chimera. Data are mean ± SD, no error estimation for groups with "zero" score. n = 4 embryos for EpiSC and n = 5 embryos for EpiSC$^{S/F}$. For each embryo, 20–60 RFP-expressing cells are scored.

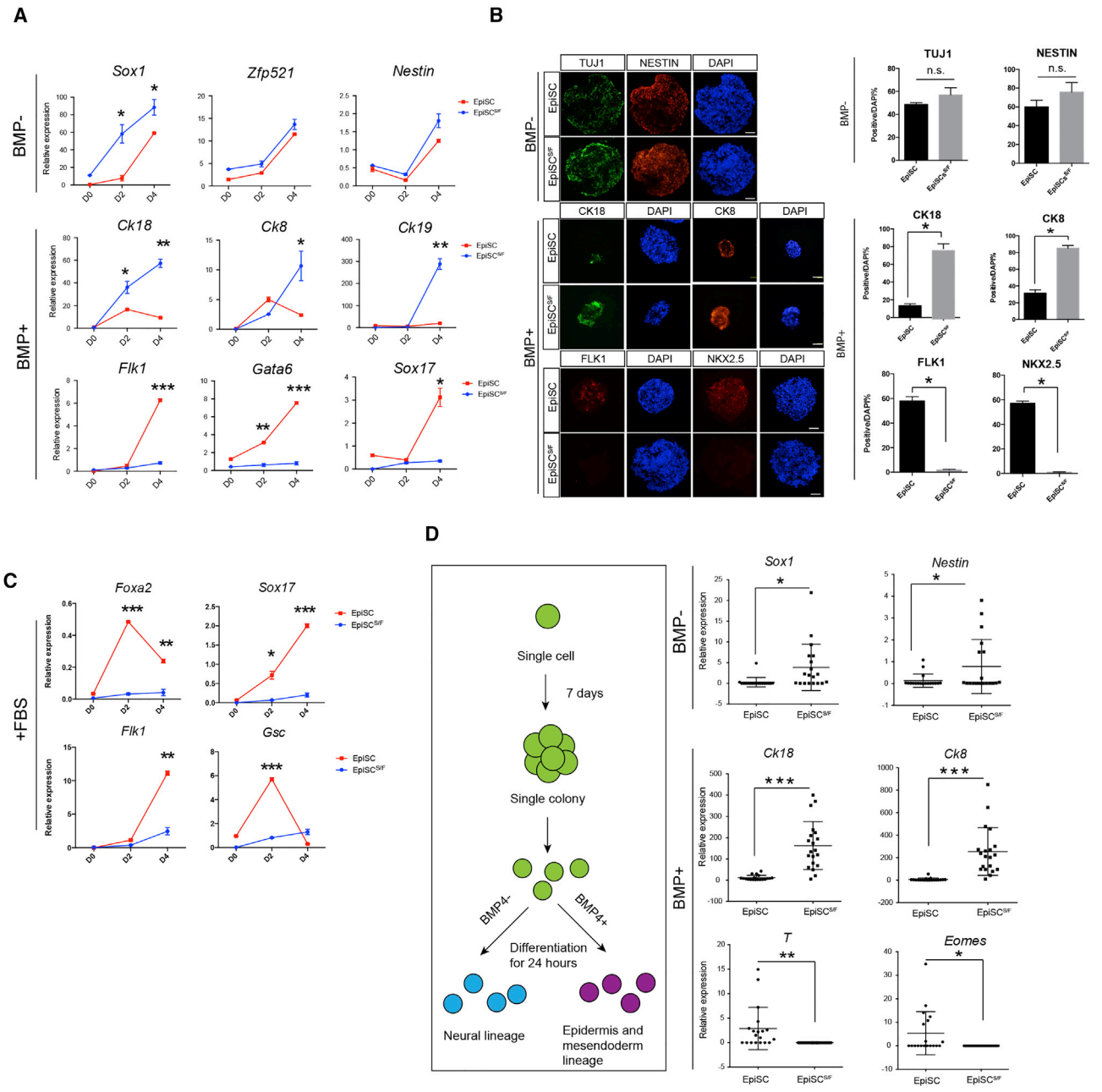

Figure 6. Differentiation of EpiSC$^{S/F}$ *In Vitro*

(A) qPCR analysis of the expression of neuroectoderm markers *Sox1*, *Zfp521*, and *Nestin*, epidermis markers *Ck18*, *Ck8*, and *Ck19*, and mesendoderm markers *Flk1*, *Gata6*, and *Sox17* during 4 days of differentiation of EpiSCs$^{S/F}$ and EpiSCs in medium with BMP4 (BMP+) and without (BMP−). Data are mean ± SD for n = 3 cultures per cell type at each time point.

(B) Immunofluorescence visualization of the expression of neuroectoderm markers TUJ1 and NESTIN, epidermis markers CK18 and CK8, and mesendoderm markers FLK1 and NKX2.5 in day-4 embryoid bodies, n = 3 cultures each for immunostaining and scoring. Data are means ± SD. Scale bars, 50 μm.

(C) qPCR analysis of the expression of the mesendoderm markers *Foxa2*, *Sox17*, *Flk1*, and *Gsc* during 4 days of differentiation of EpiSCs$^{S/F}$ and EpiSCs in fetal bovine serum-supplemented medium. Data are mean ± SD from n = 3 cultures each per cell type at each time point.

(D) Differentiation of individual descendants of a single-cell clone of EpiSC$^{S/F}$ analyzed for the expression of markers of neuroectoderm *Sox1* and *Nestin*, markers of epidermis *Ck18* and Ck8, and markers of mesendoderm *T* and *Eomes*, after 24 hr of differentiation. Twenty cells per differentiation condition were analyzed by qPCR. Data are means ± SD.

Statistical analysis was performed using Student's t tests (*p < 0.05, **p < 0.01, ***p < 0.001; n.s., not significant).

active histone profile of the promoter of surface ectoderm and epidermis genes, and the repressive profile of the promoter of mesendoderm genes. The active modifications of the promoter of neuroectoderm markers and surface ectoderm markers in the EpiSC$^{S/F}$ point to a broadly ectoderm-poised, though not neural-specific, chromatin modification. In view of that the EpiSC$^{S/F}$ can be reverted back to the EpiSC state by changing the *in vitro* conditions, it is likely that the epigenetic program of EpiSCs$^{S/F}$ may be not fixated even when they are self-renewing. In this regard, our study provides a glimpse of the interaction between extrinsic signals and the epigenome in predisposing the transcription activity that specifies the lineage propensity of EpiSCs.

In essence, our work has extended the spectrum of primed PSCs by identifying a self-renewing EpiSC population with enhanced ectoderm propensity. These ectoderm-poised EpiSCs may offer an amenable *in vitro* model, in parallel with the NPCs and the transient ectoderm progenitor cells, for investigating the mechanism of divergent specification of neuroectoderm and epidermis lineages.

EXPERIMENTAL PROCEDURES

All animal experiments were performed in accordance with the Guide of Animal Care and Use Committee of Shanghai Institute of Biochemistry and Cell Biology.

Derivation and Culture of EpiSCs$^{S/F}$

An established MEF-free EpiSC line from the Janet Rossant lab (Rugg-Gunn et al., 2012) and an EpiSC line derived from 129 strain E5.5 mouse embryo in our lab was used to generate EpiSCs$^{S/F}$. Epiblast of E5.5 129 strain mouse embryo was dissected and cultured in CDM supplemented with 20 ng/mL activin A and 10 ng/mL basic FGF (bFGF) on a feeder layer for ten passages and then cultured in feeder-free condition as stable 129 EpiSC line. EpiSCs were maintained on serum-coated plates in CDM supplemented with 20 ng/mL activin A and 10 ng/mL bFGF. To derive EpiSCs$^{S/F}$, we dissociated EpiSCs into small clumps with collagenase IV and replated them on serum-coated plates in CDM supplemented with 2 μM SB431542 and 10 ng/mL bFGF. To derive EpiSC$^{S/F}$ from single EpiSC, we dissociated EpiSCs by Accutase and plated them as single cell in 96-well plates in CDM supplemented with 2 μM SB431542 and 10 ng/mL bFGF. EpiSC$^{S/F}$ colony derived from a single EpiSC was picked up on day 8 and passaged as a cell line. EpiSCs$^{S/F}$ were passaged using collagenase IV every 2 days. EpiSC$^{S/F}$ was cryopreserved using knockout serum replacement (KSR) plus 10% DMSO and displayed similar post-thaw viability as the parental EpiSC.

RNA Preparation and Real-Time PCR

Total RNAs were extracted by using TRIzol (Invitrogen) according to the manufacturer's instructions. RNAs were reverse transcribed using SuperScript III Reverse Transcriptase (Invitrogen). Real-time PCR was performed using EvaGreen (Biotium). Expression levels of each gene were normalized to GAPDH expression and calculated by comparative C_T.

Primer Sequence

Genes	5′ Primer	3′ Primer
Rex1	CAGTTCGTCCATCTAAAAAG GGAGG	TCTTAGCTGCTTCCTTGAACAA TGCC
Oct4	AGTTGGCGTGGAGACTTTGC	CAGGGCTTTCATGTCCTGG
Nanog	TTGCTTACAAGGGTCTGCTACT	ACTGGTAGAAGAATCAGGGCT
Nodal	CCTGGAGCGCATTTGGATG	ACTTTTCTGCTCGACTGGACA
Fgf5	GCTGTGTCTCAGGGGATTGT	CACTCTCGGCCTGTCTTTTC
Sox2	GCGGAGTGGAAACTTTTGTCC	CGGGAAGCGTGTACTTATCCTT
Sox1	ATACCGCAATCCCCTCTCAG	ACAACATCCGACTCCTCTTCC
Zfp521	GAGCGAAGAGGAGTTTTTGG	AGTTCCAAGGTGGAGGTCAC
Nestin	GCTGGAACAGAGATTGGAAGG	CCAGGATCTGAGCGATCTGAC
Ck8	TCCATCAGGGTGACTCAGAAA	CCAGCTTCAAGGGGCTCAA
Ck18	CAGCCAGCGTCTATGCAGG	CTTTCTCGGTCTGGATTCCAC
Ck19	GGGGGTTCAGTACGCATTGG	GAGGACGAGGTCACGAAGC
T	CTCGGATTCACATCGTGAGAG	AAGGCTTTAGCAAATGGGTTGTA
Flk1	GGGTCGATTTCAAACCTCAATGT	AGAGTAAAGCCTATCTCGCTGT
Sox17	CGAGCCAAAGCGGAGTCTC	TGCCAAGGTCAACGCCTTC
Gata6	TTGCTCCGGTAACAGCAGTG	GTGGTCGCTTGTGTAGAAGGA
Gata4	CCCTACCCAGCCTACATGG	ACATATCGAGATTGGGGTGTCT
Eomes	CCTGGTGGTGTTTTGTTGTG	TTTAATAGCACCGGGCACTC
Klf4	CTTCAGCTATCCGATCCGGG	GAGGGGCTCACGTCATTGAT
Pax6	GCAGATGCAAAAGTCCAGGTG	CAGGTTGCGAAGAACTCTGTTT
Mixl1	ACGCAGTGCTTTCCAAACC	CCCGCAAGTGGATGTCTGG
Lefty1	CCAACCGCACTGCCCTTAT	CGCGAAACGAACCAACTTGT
Lefty2	CAGCCAGAATTTTCGAGAGGT	CAGTGCGATTGGAGCCATC
Gapdh	TGTGATGGGTGTGAACCACG AGAA	CTGTGGTCATGAGCCCTTCC ACAA

Embryonic Tissue Sample Collection

Timed-pregnant mice were euthanized for embryo collection at appropriate stages between E5.5 and E7.5. Embryos were isolated out from decidua. In all stages, Reichert's membrane and visceral endoderm was removed. Embryonic tissues were dissected by syringe needles and collected separately. E5.5 and E6.0 embryos were dissected into extraembryonic ectoderm and epiblast. E6.5 epiblast was separated into anterior (A) and posterior (P) halves. E7.0 and E7.5 epiblasts were dissected into anterior proximal (AP), anterior distal (AD), and posterior (P) fragments.

Embryonic Sample RNA-Seq and Single-Cell PCR Analysis

The tissue fragments were processed for RNA-seq or single-cell PCR analysis. In brief, single-cell or small tissue samples were lysed and reverse transcription performed (Peng et al., 2016). After the first-strand synthesis, cDNA was preamplified with KAPA HiFi Hotstart ReadyMix (KAPA Biosystems) by IS-PCR primer for 18 cycles. cDNA quality was assessed by qPCR examination of several housekeeping genes.

qPCR was then performed on single-cell preamplified cDNAs. For embryonic samples, cDNA was further verified by examining representative known position markers such as *Sox2* and *T* to ascertain correct tissue dissection and adequate preamplification.

For sequencing library construction, cDNA was purified using a 1:0.8 ratio of AMPure XP beads (Beckman Coulter). After quantification by Qubit, cDNA was applied to Bioanalyzer 2100 on a High-Sensitive DNA chip (Agilent Bioanalyzer) to check the library size distribution. Amplified cDNA (~5 ng) was then used to construct Illumina sequencing libraries using Illumina's Nextera DNA sample preparation kit following the manufacturer's recommended manual. All sample libraries were sequenced on an Illumina HiSeq2000 machine with at least 20 million cleaned reads. The sequencing was performed by Berry Genomics (Beijing, China).

RNA-Seq Data Processing

Raw reads were mapped to mm10 using the TopHat version 2.0.13 program (Trapnell et al., 2009). We assigned FPKM (fragments per kilobase per million) as an expression value for each gene using Cufflinks version 1.3.0 software (Trapnell et al., 2010). Cuffdiff software was then used to identify differentially expressed genes between treatment and control samples (Trapnell et al., 2013). Differentially expressed gene heat maps were clustered by hierarchical clustering and visualized using Java TreeView software (Saldanha, 2004). PCA analysis was performed using R (http://www.r-project.org). Pearson correlation was used to compare cell lines with *in vivo* isolated embryonic tissue.

In Vitro Differentiation

EpiSCs and EpiSCs$^{S/F}$ were differentiated into EBs in KSR medium (Glasgow minimal essential medium supplemented with 8% KSR, 2 mM glutamine, 1 mM pyruvate, 0.1 mM nonessential amino acids, and 0.1 mM 2-mercaptoethanol) and KSR medium plus 10 ng/mL BMP4, respectively. RNA samples were collected every 2 days and analyzed by qPCR. For single-cell differentiation, EpiSCs$^{S/F}$ and EpiSCs were cultured singly for 7 days followed by the dissociation of the resultant clones into single cells. The single-cell suspension of each clone was split into two aliquots, with one used for neural differentiation (KSR medium without BMP4) and the other for epidermis and mesoderm differentiation (induced by 10 ng/mL BMP4). After differentiation *in vitro* for 24 hr, 20 single cells were collected from each culture and analyzed by qPCR.

Grafting and *In Vitro* Embryo Culture

RFP-expressing *PB* (*PGK-neo*) and *ACT-PBase* plasmids (Yang et al., 2013) were co-transfected into cells by Lipofectamine (Invitrogen) to label the cell with RFP. RFP-expressing EpiSCs and EpiSCs$^{S/F}$ were tested for their germ-layer differentiation potential by grafting ~10 cells to the anterior and posterior sites of host ICR E6.5 and E7.0 embryos. Cells were dispersed into clumps using collagenase and collected for grafting. The engrafted host embryos were cultured in heat-inactivated rat serum under 5% oxygen, 5% carbon dioxide, and 90% nitrogen at 37°C for 48 hr (E6.5 chimeras) or 24 hr (E7.0 chimeras). After *in vitro* culture, the embryo was photographed to record the distribution of the grafted cells by fluorescence microscopy. The yolk sac and amnion were dissected away, the embryos were fixed in 4% paraformaldehyde for 1hr, and the embryos were embedded in OCT compound and cryosectioned.

Immunofluorescence

For immunofluorescence, cells were fixed with freshly prepared 4% paraformaldehyde in PBS for 0.5 hr at room temperature. Fixed cells and chimeric embryo cryosections were treated with blocking buffer (PBS containing 0.3% Triton X-100, 5% BSA, and 0.5% normal goat serum) for 2 hr at room temperature. The cells and sections were incubated with primary antibodies in blocking buffer overnight at 4°C. The next day, cells and sections were washed and incubated with fluorescent-labeled secondary antibodies at 1:500 dilutions for 1 hr at room temperature. The cells and sections were stained with DAPI and mounted in Mowiol mounting medium. Specimens were observed with a Leica TCS SP5 confocal microscope. Primary antibodies used in this study include: Oct3/4 (1:200, Santa Cruz Biotechnology, sc-5279), T (1:200, R&D Systems, AF2085), Sox2 (1:100, Abcam, ab59776), Nanog (1:200, CST, 8822), Fgf5 (1:50, Santa Cruz, sc-7914), Tuj1 (1:400, BioLegend, 801201), Nestin (1:100, made by our lab), Ck18 (1:100, Abcam, ab668), Flk1 (1:100, Becton Dickinson, 561993), Nkx2.5 (1:200, Santa Cruz, sc-8697), Tbx6 (1:100, Abcam, ab38883), and Foxa2 (1:100, Abcam, ab23630).

Chromatin Immunoprecipitation

Chromatin immunoprecipitation (ChIP) experiments were carried out as described by Qiao et al. (2015). In brief, cells were collected and fixed in 1% formaldehyde solution and quenched by 0.125 M glycine. Fixed cells were fragmented to a size range of 200–500 bp by using Bioruptor Pico. Solubilized fragmented chromatin was immunoprecipitated with antibodies against H3K4me3 (Abcam, 8580), H3K27me3 (Millipore, 07-449), and H3K27ac (Active Motif, 39133). Antibody-chromatin complexes were pulled down using protein G beads (Dynabeads, 10004D), washed several times, and eluted. Reverse crosslink was performed subsequently under 65°C for at least 4 hr. Chromatin mixture solution was treated with RNase A and proteinase K to remove residual RNAs and proteins. Finally, fragmented DNA was extracted with phenol-chloroform and precipitated with ethanol. ChIP DNA was finally dissolved in nuclease-free water and quantified using Qubit. DNA fragments acquired from immunoprecipitation would be subjected to end-repaired, adaptor ligation, and PCR amplification under the instruction of the manufacturers (New England Biolabs, E7370).

ChIP-Seq Data Processing

Raw reads were mapped to mm10 using Bowtie2 version 2.2.2 (Langmead and Salzberg, 2012). MACS2 version 2.1.1.20160309

was used to call ChIP sequencing (ChIP-seq) peaks using broad peak calling mode (with –broad option), as well as to identify differential ChIP-seq signals in different conditions (Zhang et al., 2008). ChIPseeker (Yu et al., 2015) was used to annotate ChIP-seq peaks by using the mouse gene annotation GENCODE version M9. deepTools (Ramirez et al., 2014) was used to smooth and calculate the ChIP-seq signal as the ratio between ChIP-seq data and corresponding input control data, as well as to visualize ChIP-seq signals.

Statistics

Each experiment was performed at least three times. The data are presented as the mean ± SD. Student's t test was used to compare the effects of all treatments. Statistically significant differences are indicated in the figures as follows: *$p < 0.05$, **$p < 0.01$, and ***$p < 0.001$.

ACCESSION NUMBERS

All RNA-seq data and ChIP-seq data are available at the Gene Expression Omnibus under accession number GEO: GSE92635.

SUPPLEMENTAL INFORMATION

Supplemental Information includes five figures and can be found with this article online at https://doi.org/10.1016/j.stemcr.2018.05.019.

AUTHOR CONTRIBUTIONS

N.J., C.L., and P.P.L.T. designed the project; C.L., X.Y., J.C., G.C., W.G., Y.C., and P.O. conducted the experiments; Z.H., R.W., P.O., and E.W. performed the bioinformatics analysis; C.L., G.P., P.P.L.T., and N.J. analyzed the data and wrote the paper.

ACKNOWLEDGMENTS

We thank Dr. Janet Rossant for providing the EpiSC line and Dr. Jinsong Li for providing the PB (PGK-neo) and ACT-PBase plasmid. This work was supported in part by the "Strategic Priority Research Program" of the Chinese Academy of Sciences (grant no. XDA16020501 to N.J., XDA16020404 to G.P.), the National Key Basic Research and Development Program of China (2017YFA0102700, 2015CB964500, 2014CB964804), the National Natural Science Foundation of China (31661143042, 91519314, 31630043, 31571513, 31430058), the National Health and Medical Research Council (NHMRC) of Australia (632776), and the Australian Research Council (DP 160100933). P.O. was supported by the Fondation pour la Recherche Medicale (FRM SPE20140129375). P.P.L.T. is an NHMRC Senior Principal Research Fellow (grants 1003100, 1110751).

Received: October 9, 2017
Revised: May 27, 2018
Accepted: May 28, 2018
Published: June 28, 2018

REFERENCES

Brennan, J., Lu, C.C., Norris, D.P., Rodriguez, T.A., Beddington, R.S., and Robertson, E.J. (2001). Nodal signalling in the epiblast patterns the early mouse embryo. Nature *411*, 965–969.

Brons, I.G., Smithers, L.E., Trotter, M.W., Rugg-Gunn, P., Sun, B., Chuva de Sousa Lopes, S.M., Howlett, S.K., Clarkson, A., Ahrlund-Ritcher, L., Pederson, R.A., et al. (2007). Derivation of pluripotent epiblast stem cells from mammalian embryos. Nature *448*, 191–195.

Buecker, C., Srinivasan, R., Wu, Z., Calo, E., Acampora, D., Faial, T., Simeone, A., Tan, M., Swigut, T., and Wysocka, J. (2014). Reorganization of enhancer patterns in transition from naive to primed pluripotency. Cell Stem Cell *14*, 838–853.

Cajal, M., Lawson, K.A., Hill, B., Moreau, A., Rao, J.G., Ross, A., and Camus, A. (2012). Clonal and molecular analysis of the prospective anterior neural boundary in the mouse embryo. Development *139*, 423–436.

Camus, A., Perea-Gomez, A., Moreau, A., and Collignon, J. (2006). Absence of Nodal signaling promotes precocious neural differentiation in the mouse embryo. Dev. Biol. *295*, 743–755.

Conlon, F.L., Lyons, K.M., Takaesu, N., Barth, K.S., Kispert, A., Herrmann, B., and Robertson, E.J. (1994). A primary requirement for nodal in the formation and maintenance of the primitive streak in the mouse. Development *120*, 1919–1928.

Evans, M.J., and Kaufman, M.H. (1981). Establishment in culture of pluripotential cells from mouse embryos. Nature *292*, 154–156.

Gao, X., and Hannoush, R.N. (2014). Single-cell imaging of Wnt palmitoylation by the acyltransferase porcupine. Nat. Chem. Biol. *10*, 61–68.

Hayashi, K., Ogushi, S., Kurimoto, K., Shimamoto, S., Ohta, H., and Saitou, M. (2012). Offspring from oocytes derived from in vitro primordial germ cell-like cells in mice. Science *338*, 971–975.

Huang, Y., Osorno, R., Tsakiridis, A., and Wilson, V. (2012). In Vivo differentiation potential of epiblast stem cells revealed by chimeric embryo formation. Cell Rep. *2*, 1571–1578.

Huelsken, J., Vogel, R., Brinkmann, V., Erdmann, B., Birchmeier, C., and Birchmeier, W. (2000). Requirement for beta-catenin in anterior-posterior axis formation in mice. J. Cell Biol. *148*, 567–578.

Kimura-Yoshida, C., Nakano, H., Okamura, D., Nakao, K., Yonemura, S., Belo, J.A., Aizawa, S., Matsui, Y., and Matsuo, I. (2005). Canonical Wnt signaling and its antagonist regulate anterior-posterior axis polarization by guiding cell migration in mouse visceral endoderm. Dev. Cell *9*, 639–650.

Kojima, Y., Kaufman-Francis, K., Studdert, J.B., Steiner, K.A., Power, M.D., Loebel, D.A., Jones, V., Hor, A., de Alencastro, G., Logan, G.J., et al. (2014). The transcriptional and functional properties of mouse epiblast stem cells resemble the anterior primitive streak. Cell Stem Cell *14*, 107–120.

Langmead, B., and Salzberg, S.L. (2012). Fast gapped-read alignment with Bowtie 2. Nat. Methods *9*, 357–359.

Lewis, S.L., Khoo, P.L., De Young, R.A., Steiner, K., Wilcock, C., Mukhopadhyay, M., Westphal, H., Jamieson, R.V., Robb, L., and Tam,

P.P. (2008). Dkk1 and Wnt3 interact to control head morphogenesis in the mouse. Development *135*, 1791–1801.

Li, L., Liu, C., Biechele, S., Zhu, Q., Song, L., Lanner, F., and Rossant, J. (2013). Location of transient ectodermal progenitor potential in mouse development. Development *140*, 4533–4543.

Li, L., Song, L., Liu, C., Chen, J., Peng, G., Wang, R., Liu, P., Tang, R., Rossant, J., and Jing, N. (2015). Ectodermal progenitors derived from epiblast stem cells by inhibition of Nodal signaling. J. Mol. Cell Biol. *7*, 455–465.

Li, W., Sun, W., Zhang, Y., Wei, W., Ambasudhan, R., Xia, P., Talantova, M., Lin, T., Kim, J., Wang, X., et al. (2011). Rapid induction and long-term self-renewal of primitive neural precursors from human embryonic stem cells by small molecule inhibitors. Proc. Natl. Acad. Sci. USA *108*, 8299–8304.

Liu, P., Wakamiya, M., Shea, M.J., Albrecht, U., Behringer, R.R., and Bradley, A. (1999). Requirement for Wnt3 in vertebrate axis formation. Nat. Genet. *22*, 361–365.

Lu, C.C., Brennan, J., and Robertson, E.J. (2001). From fertilization to gastrulation: axis formation in the mouse embryo. Curr. Opin. Genet. Dev. *11*, 384–392.

Martin, G.R. (1981). Isolation of a pluripotent cell line from early mouse embryos cultured in medium conditioned by teratocarcinoma stem cells. Proc. Natl. Acad. Sci. USA *78*, 7634–7638.

Mascetti, V.L., and Pedersen, R.A. (2016). Human-mouse chimerism validates human stem cell pluripotency. Cell Stem Cell *18*, 67–72.

Mesnard, D., Guzman-Ayala, M., and Constam, D.B. (2006). Nodal specifies embryonic visceral endoderm and sustains pluripotent cells in the epiblast before overt axial patterning. Development *133*, 2497–2505.

Mukhopadhyay, M., Shtrom, S., Rodriguez-Esteban, C., Chen, L., Tsukui, T., Gomer, L., Dorward, D.W., Glinka, A., Grinberg, A., Huang, S.P., et al. (2001). Dickkopf1 is required for embryonic head induction and limb morphogenesis in the mouse. Dev. Cell *1*, 423–434.

Patani, R., Compston, A., Puddifoot, C.A., Wyllie, D.J., Hardingham, G.E., Allen, N.D., and Chandran, S. (2009). Activin/Nodal inhibition alone accelerates highly efficient neural conversion from human embryonic stem cells and imposes a caudal positional identity. PLoS One *4*, e7327.

Peng, G., Suo, S., Chen, J., Chen, W., Liu, C., Yu, F., Wang, R., Chen, S., Sun, N., Cui, G., et al. (2016). Spatial transcriptome for the molecular annotation of lineage fates and cell identity in mid-gastrula mouse embryo. Dev. Cell *36*, 681–697.

Perea-Gomez, A., Vella, F.D., Shawlot, W., Oulad-Abdelghani, M., Chazaud, C., Meno, C., Pfister, V., Chen, L., Robertson, E., Hamada, H., et al. (2002). Nodal antagonists in the anterior visceral endoderm prevent the formation of multiple primitive streaks. Dev. Cell *3*, 745–756.

Pfister, S., Steiner, K.A., and Tam, P.P. (2007). Gene expression pattern and progression of embryogenesis in the immediate post-implantation period of mouse development. Gene Expr. Patterns *7*, 558–573.

Qiao, Y., Wang, X., Wang, R., Li, Y., Yu, F., Yang, X., Song, L., Xu, G., Chin, Y.E., and Yang, X. (2015). AF9 promotes hESC neural differentiation through recruiting TET2 to neurodevelopmental gene loci for methylcytosine hydroxylation. Cell Discov. *1*, 15017.

Ramirez, F., Dundar, F., Diehl, S., Gruning, B.A., and Manke, T. (2014). deepTools: a flexible platform for exploring deep-sequencing data. Nucleic Acids Res. *42* (Web Server issue), W187–W191.

Rugg-Gunn, P.J., Cox, B.J., Lanner, F., Sharma, P., Ignatchenko, V., McDonald, A.C., Garner, J., Gramolini, A.O., Rossant, J., and Kislinger, T. (2012). Cell-surface proteomics identifies lineage-specific markers of embryo-derived stem cells. Dev. Cell *22*, 887–901.

Saldanha, A.J. (2004). Java Treeview-extensible visualization of microarray data. Bioinformatics *20*, 3246–3248.

Smith, J.R., Vallier, L., Lupo, G., Alexander, M., Harris, W.A., and Pedersen, R.A. (2008). Inhibition of Activin/Nodal signaling promotes specification of human embryonic stem cells into neuroectoderm. Dev. Biol. *313*, 107–117.

Tam, P.P. (1989). Regionalisation of the mouse embryonic ectoderm: allocation of prospective ectodermal tissues during gastrulation. Development *107*, 55–67.

Tam, P.P.L., and Loebel, D.A.F. (2007). Gene function in mouse embryogenesis: get set for gastrulation. Nat. Rev. Genet. *8*, 368–381.

Tesar, P.J., Chenoweth, J.G., Brook, F.A., Davies, T.J., Evans, E.P., Mack, D.L., Gardner, R.L., and McKay, R.D. (2007). New cell lines from mouse epiblast share defining features with human embryonic stem cells. Nature *448*, 196–199.

Trapnell, C., Hendrickson, D.G., Sauvageau, M., Goff, L., Rinn, J.L., and Pachter, L. (2013). Differential analysis of gene regulation at transcript resolution with RNA-seq. Nat. Biotechnol. *31*, 46–53.

Trapnell, C., Pachter, L., and Salzberg, S.L. (2009). TopHat: discovering splice junctions with RNA-seq. Bioinformatics *25*, 1105–1111.

Trapnell, C., Williams, B.A., Pertea, G., Mortazavi, A., Kwan, G., van Baren, M.J., Salzberg, S.L., Wold, B.J., and Pachter, L. (2010). Transcript assembly and quantification by RNA-seq reveals unannotated transcripts and isoform switching during cell differentiation. Nat. Biotechnol. *28*, 511–515.

Vallier, L., Mendjan, S., Brown, S., Chng, Z., Teo, A., Smithers, L.E., Trotter, M.W., Cho, C.H., Martinez, A., Rugg-Gunn, P., et al. (2009). Activin/Nodal signalling maintains pluripotency by controlling Nanog expression. Development *136*, 1339–1349.

Vallier, L., Reynolds, D., and Pedersen, R.A. (2004). Nodal inhibits differentiation of human embryonic stem cells along the neuroectodermal default pathway. Dev. Biol. *275*, 403–421.

Wu, J., Okamura, D., Li, M., Suzuki, K., Luo, C.Y., Ma, L., He, Y., Li, Z., Benner, C., Tamura, I., et al. (2015). An alternative pluripotent state confers interspecies chimaeric competency. Nature *521*, 316–321.

Yang, H., Liu, Z., Ma, Y., Zhong, C., Yin, Q., Zhou, C., Wang, H., Tang, F., Wang, Y., Zhang, C., et al. (2013). Generation of haploid embryonic stem cells from *Macaca fascicularis* monkey parthenotes. Cell Res. *23*, 1187–1200.

Yu, G., Wang, L.G., and He, Q.Y. (2015). ChIPseeker: an R/Bioconductor package for ChIP peak annotation, comparison and visualization. Bioinformatics *31*, 2382–2383.

Zhang, K., Li, L., Huang, C., Shen, C., Tan, F., Xia, C., Liu, P., Rossant, J., and Jing, N. (2010). Distinct functions of BMP4 during different stages of mouse ES cell neural commitment. Development *137*, 2095–2105.

Zhang, Y., Liu, T., Meyer, C.A., Eeckhoute, J., Johnson, D.S., Bernstein, B.E., Nusbaum, C., Myers, R.M., Brown, M., Li, W., et al. (2008). Model-based analysis of ChIP-Seq (MACS). Genome Biol. *9*, R137.

Zhu, Q., Song, L., Peng, G., Sun, N., Chen, J., Zhang, T., Sheng, N., Tang, W., Qian, C., Qiao, Y., et al. (2014). The transcription factor Pou3f1 promotes neural fate commitment via activation of neural lineage genes and inhibition of external signaling pathways. Elife *3*. https://doi.org/10.7554/eLife.02224.